Twodimensional equilibria of fieldreversed configurations in a perfectly conducting cylindrical shell

D. W. Hewett and R. L. Spencer

Citation: Physics of Fluids (1958-1988) **26**, 1299 (1983); doi: 10.1063/1.864291
View online: http://dx.doi.org/10.1063/1.864291
View Table of Contents: http://scitation.aip.org/content/aip/journal/pof1/26/5?ver=pdfcov
Published by the AIP Publishing

Two-dimensional equilibria of field-reversed configurations in a perfectly conducting cylindrical shell

D. W. Hewett and R. L. Spencer
Los Alamos National Laboratory, Los Alamos, New Mexico 87545

(Received 1 September 1982; accepted 13 December 1982)

Two-dimensional field-reversed equilibria bounded by a conducting cylinder are computed. The computation is made possible by using a global constraint and by using a computational algorithm that is protective of the initial guess. A pressure profile is used that has sufficient generality to match experimentally produced configurations. It is found that for some choices of separatrix radius and separatrix beta, no equilibria exist. The reasons for loss of equilibrium are discussed and an example of a configuration near loss of equilibrium conditions is given.

I. INTRODUCTION

Elongated equilibria are commonly observed in field-reversed theta-pinch experiments.[1-5] These plasmas are relatively hot (500–1000 eV) and dense (10^{15} cm^{-3}) and last for many Alfvén transit times before they terminate. This evidence of macroscopic stability together with the possibility of good confinement because of closed magnetic field lines makes these configurations quite interesting to the magnetic fusion community. The purpose of this work is to understand what sort of time-independent states are possible and to identify the parameters that characterize these states. An appropriate computational model must first be chosen. Because much of the plasma in such a configuration is in a region of very low magnetic field, many of the ion orbits are much larger than gradient scale lengths. Were the ions to carry current, the ion pressure would have to be represented by a tensor with off-diagonal elements and the equilibrium problem would be quite difficult. In particular, the magnetohydrodynamic (MHD) model would be inappropriate. If, however, the ions carry no current and are confined electrostatically by an electric potential that is constant on flux surfaces, then the ion pressure can be represented by a scalar and MHD is a valid model. It is assumed in what follows that these conditions are met.

The computation of elongated field-reversed configuration (FRC) equilibria has tuned out to be surprisingly difficult even with the MHD model. The simplest realistic equilibrium is the prolate Hill's vortex with a vacuum field outside the separatrix.[6] Unfortunately this solution has an elliptical separatrix that is quite unlike the racetrack-shaped separatrix configuration observed in experiments. Another objection is that these states have rather odd-shaped flux surfaces outside the separatrix implying external coils significantly more complicated than the cylindrical conducting shell of experiments. A more general analytic solution is that of Berk, Hammer, and Weitzner,[7] which has been numerically implemented and extended by Anderson, Hammer, and Barnes.[8] These equilibria have a separatrix shape more like those observed in experiments but the vacuum field outside the separatrix does not have straight field lines at the conducting wall. A more successful calculation is that of Semenov and Sosnin; they use power law pressure profiles and their equilibria do have straight field lines at the conducting wall.[9] Recently, a simplified model by Spencer and Hewett[10] revealed some of the pathologies of elongated FRC equilibria that have contributed to the difficulty of commuting such states.

The ideas presented here are based on this recent work and overcome several stumbling blocks encountered by earlier research. In Sec. II the numerical difficulties encountered by Spencer and Hewett are reviewed with an eye towards the requirements of a successful Grad–Shafranov solution technique—discussed in Sec III. The resulting algorithm allows the computation of elongated field-reversed equilibria—examples of which are presented in Sec. IV. Loss of equilibrium is also discussed. The paper is concluded with a short discussion and summary in Sec. V.

II. THE PRESSURE PROFILE $p(\psi) = C\psi H(\psi)$

The work to be presented in later sections of this paper owes its success to the understanding of the 2- and 1-D states for $p'(\psi) = CH(\psi)$, where $p(\psi)$ is the plasma pressure as a function of the magnetic flux function ψ, C is a constant, $H(\psi)$ is a Heaviside function ($H = 1$ for $\psi < 0$, $H = 0$ for $\psi > 0$), and the prime denotes differentiation with respect to ψ. As is discussed later, this rather specialized $p(\psi)$ provides generic guidance for most physically realistic choices for $p(\psi)$.

Equilibriuim requires that the flux function ψ satisfy the Grad–Shafranov equation

$$\Delta^*\psi \equiv r\frac{\partial}{\partial r}\left(\frac{1}{r}\frac{\partial\psi}{\partial r}\right) + \frac{\partial^2\psi}{\partial z^2} = -r^2p'(\psi), \tag{1}$$

where

$$B_r = -\frac{1}{r}\frac{\partial\psi}{\partial z}, \quad B_z = \frac{1}{r}\frac{\partial\psi}{\partial r}.$$

It is assumed that $B_{\text{toroidal}} \equiv 0$. A further assumption is that $\psi = \psi_w$ at $r = r_w$, where the subscript w denotes evaluation at the wall position. This is a perfectly conducting wall boundary condition.

An understanding of some difficulties that must be avoided in 2-D can be gained by considering the z-independent states. Following Spencer and Hewett,[10] there is one purely vacuum state (no plasma; ψ everywhere positive) and there are two 1-D plasma states—states having reversed magnetic field on axis but with sufficient positive field on the

 0031-9171/83/051299-06$01.90

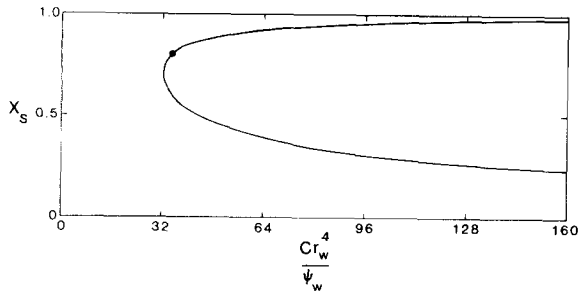

FIG. 1. The radial separatrix position $x_s = r_s/r_w$ for 1-D equilibria as a function of the parameter C in the Heaviside pressure profile.

outside so that the total flux is positive. For values of $C > 32\psi_w/r_w^4$, these two z-independent plasma states have distinct separatrix ($\psi = 0$) radii (see Fig. 1). The axial pressure balance condition[1,11] now provides further guidance on this point. The conditions that a very long 2-D equilibrium be in axial force balance can be satisfied at only one point on the curve of $x_s = r_s/r_w$ vs C—namely on the upper branch at $C = C_2 = 36\,\psi_w/r_w^4$. Highly elongated 2-D states must have $C = C_2$ to satisfy axial pressure balance.

The 2-D Heaviside results now provide crucial insight into the selection of a parameter for labeling equilibria. The separatrix approaches a spherical shape for large C. As C is decreased the separatrix becomes elongated in the axial direction with the elongation becoming an extremely sensitive function of C as it nears C_2. The elongation varies from $2-\infty$ as C varies from $1.003C_2$–C_2, respectively. Choosing C is thus a poor way to specify long equilibria. A much better way would be to choose a parameter that depends strongly on the length of the equilibrium. The total toroidal current in the computational region I_θ is such a parameter. Using it to specify equilibria gives the added advantage that two of the three 1-D states allowed when C is used are eliminated. For example, consider the plot of toroidal current per unit length J_θ displayed as Fig. 2 for the Heaviside profile. For a given value of C there are equilibria with two values of J_θ plus the vacuum state with $J_\theta = 0$. But if J_θ is specified, the one equilibrium with $J_\theta = I_\theta/L$, L the length of the computation region, is selected. Using I_θ instead of C thus better determines the equilibrium length and reduces the number of allowed equilibria.

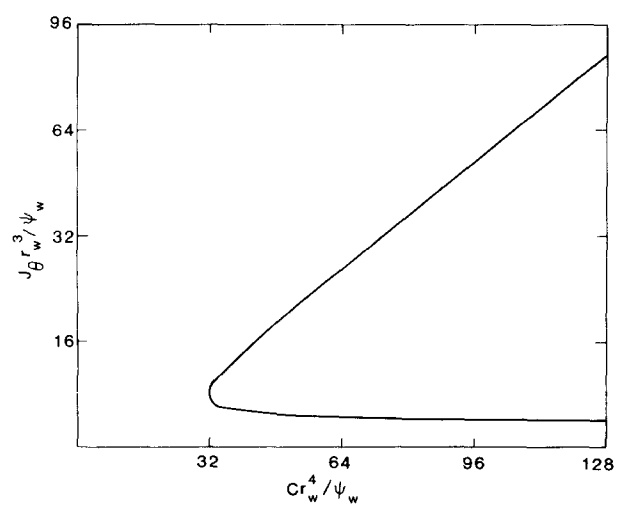

FIG. 2. The toroidal current j_θ per unit length in 1-D states as a function of the parameter C in the Heaviside pressure profile.

III. NUMERICAL SOLUTION

The numerical solution of this equilibrium problem has proven to be unexpectedly difficult. One successful approach is presented here. A brief discussion of unsuccessful approaches is also useful as an aid to understanding the requirements of a successful procedure. Other methods that promise to reduce the computational effort required are currently being investigated.

The first approach was to try to obtain a finite difference solution of Eq. (1) with simple successive over-relaxation (SOR). The finite difference representation of Eq. (1) is

$$\frac{r_i}{\Delta r^2}\left(\frac{\psi_{i+1,j}-\psi_{i,j}}{r_{i+1/2}} - \frac{\psi_{i,j}-\psi_{i-1,j}}{r_{i-1/2}}\right) + \frac{\psi_{i,j+1}-2\psi_{i,j}+\psi_{i,j-1}}{\Delta z^2} = -r_i^2 p'(\psi_{i,j}), \tag{2}$$

where $\psi_{i,j}$ is the value of ψ at the position r_i and z_j. Δr and Δz are uniform grid sizes in r and z. SOR can the represented schematically by

$$\psi_{i,j}^{n+1} = \omega\tilde{\psi}_{i,j} + (1-\omega)\psi_{i,j}^n, \tag{3}$$

where the superscript is the iteration number, ω is the relaxation parameter, and $\tilde{\psi}$ is the algebraic solution of Eq. (2) for $\psi_{i,j}$ using the most recently updated values for the required neighbors. Solutions obtained were always 1-D states—possibly due to poor initial guesses for the desired 2-D solutions—and were extremely expensive in CPU time. Since 2-D equilibria having proper conducting wall boundary conditions were the goal of this work, time requirements were of secondary importance initially—allowing other even more conservative (slower) convergence schemes to be tried. A promising idea was to substitute iteration schemes involving more than one previous iteration level for the simple-SOR-Picard scheme, Eq. (3). The scheme of Marder and Weitzner,[12]

$$\psi_{i,j}^{n+1} = -\omega\tilde{\psi}_{i,j} + 2\omega\psi_{i,j}^n + (1-\omega)\psi_{i,j}^{n-1}, \tag{4}$$

is one of several variables that have the property of turning some unstable iteration schemes into stable ones. Our implementation of these schemes was unsuccessful in finding 2-D equilibria for this highly nonlinear free-boundary problem. It is believed that the essential weakness of these schemes lies in the difficulty of selecting acceleration parameters (analogous to ficticious time steps towards an asymptotic state) that allow reasonable convergence without iteration slipping off to any of the 1-D states that are more stable to iteration.

A solution to these difficulties is to use an algorithm that adaptively selects the acceleration parameter. Such a procedure is "protective" of the initial guess in that if a step were to deviate too much from the last iterate, the proposed iterate is discarded and the step is reduced for the next attempt. The method used for the successful generation of 2-D states is based on the original ideas of Doss and Miller[13] and

is now briefly described.

The procedure of Doss and Miller allows the dynamic selection of an acceleration parameter ω for a relatively standard alternating direction implicit (ADI) procedure. The basic alternating direction implicit (ADI) iteration is defined by expressing the operator in Eq. (2) in two parts. Separating in r and z derivatives, Eq. (2) becomes

$$\omega\psi^{n+1/2} - D_r(\psi^{n+1/2}) = \omega\psi^n + D_z(\psi^n), \tag{5a}$$

$$\omega\psi^{n+1} - D_z(\psi^{n+1}) = \omega\psi^{n+1/2} + D_r(\psi^{n+1/2}), \tag{5b}$$

where D_r (D_z) represents the r-(z-)differential operator. As represented by Eqs. (5a) and (5b), an iteration is accomplished in two half steps—each being semi-implicit. The extension that provides for dynamic determination of ω is to compare the norms

$$N = \sum_i \sum_j (\psi^{n+1} - \psi^n)^2,$$

and

$$N_* = \sum_i \sum_j (\psi_*^{n+1} - \psi^{n+1})^2,$$

where ψ_*^{n+1} represents the result of a double application of Eqs. 5 with twice the ω. Small N_* reflects adequate convergence in iteration "time step"; finite N quantifies the movement toward the asymptotic state. The ratio N_*/N determines a multiplicative factor, $0.1 \leqslant f \leqslant 2$, used to modify the ω for the next iteration.[14] The concept is that idealized iteration should exhibit change from the initial state (finite N) that is always larger than the variation (N_*) arising from adjustments in the iteration "time step." A mapping is selected for N_*/N to f which continually adjusts the acceleration parameter ω so that N_*/N usually falls betweeen 0.02 and 0.4. Experience suggests that optimal security and convergence are obtained in the high end of this range. Details of this elliptic solution technique applied to other problems can be found in the original reference.[13]

A most important "protective" feature that is perhaps essential for this highly nonlinear application is that the algorithm provides for the complete rejection of the newly proposed iterate ψ_*^{n+1} should the ratio of the two norms get too large ($N_*/N > 0.4$). Conversely, should the ratio become too small ($N_*/N < 0.02$), the indication is that the iteration is taking an excessive number of steps; ω is reduced by a factor $f = 10.0$ in these cases. The principal advantage this provides is that given a crude but strongly 2-D initial guess, the algorithm must be sufficiently conservative so that "large" steps do not allow the solution to "radically" shift to the 1-D plasma state. At other instances in the process, a much smaller ω provides desirable convergence enhancements. The above procedure provides rapid convergence for a wide variety of linear and nonlinear problems.

An added complication in the present problem is that a global constraint must be satisfied. The global constraint I_θ is implemented by defining the constant C in the p' function, $p' = CS(\psi)$, after each iteration so that the I_θ is preserved. In this notation the function $S(\psi)$ contains the functional dependence on ψ. Since $J_\theta = rp'$, I_θ is given by

$$I_\theta = C \int_0^{r_w} dr \int_0^{z_{\max}} dz\, rS[\psi(r,z)],$$

where $z_{\max}$ is the length of the computation region, resulting in the redefinition after each application of Eqs. (5)

$$C^{n+1} = I_\theta \left(C^n \int_0^{r_w} dr \int_0^{z_{\max}} dr\, rS[\psi^{n+1}(r,z)] \right)^{-1}. \tag{6}$$

The result is that, on each iteration, the right-hand side p' changes not only because ψ has changed but also because the constant C has been changed; I_θ is, thus, preserved as a global constraint.

As discussed in the preceding section, the global constraint reduces the number of states that must be considered by restricting the possible configurations to those that have the desired current. The solution is further restricted by the boundary conditions. The flux function is required to vanish at $r = 0$ and to be equal to ψ_w at $r = r_w$. It is required to satisfy $\partial\psi/\partial z = 0$ in the midplane and at $z = z_{\max}$. These are the simplest boundary conditions consistent with experiments. Other conditions, like the presence of external magnetic mirrors, have been added by altering these boundary conditions.

IV. RESULTS

Several cases were run with the Heaviside $p(\psi)$ profile. A typical example is shown in Fig. 3. This particular example has an elongation $\epsilon = z_s/r_s$ of approximately five where z_s (r_s) is the coordinate of the intersection of the separatrix, $\psi = 0$, with the $r = 0$ ($z = 0$) boundary. The shape of the separatrix for $\epsilon \geqslant 2$ is, to good approximation, z independent near $z = 0$. Straight field line regions at the midplane and beyond $z = z_s$ are joined by a transition region around $z = z_s$. As I_θ is decreased, z_s decreases with r_s approximately fixed until $\epsilon \simeq 1$; as I_θ is decreased further, the separatrix maintains a spherical shape with the radius shrinking to zero. These results, obtained with the numerical technique described in Sec. III, agree with the semianalytic results of Spencer and Hewett.[10]

Several more general expressions for $p(\psi)$ have also been considered that have more freedom to match experimental data. Any $p(\psi)$ that has finite pressure for negative ψ regions, relatively small pressure for positive ψ, and a smooth transition with large p' near $\psi = 0$ is potentially of interest. Profiles $p(\psi)$ with these properties will produce equilibria with the same general properties as the Heaviside profile discussed in Sec. II. Consequently, the total toroidal current I_θ remains a useful free parameter for these generic profiles.

A quite general choice for the pressure profile is

$$S(\psi) = d_1 \operatorname{sech}^2(a_1\psi - b_1). \tag{7}$$

Note that d_1, like C, is not fixed; its determination is part of the solution to the equilibrium problem. This profile will be referred to as the SECH profile. The extra parameters in Eq.

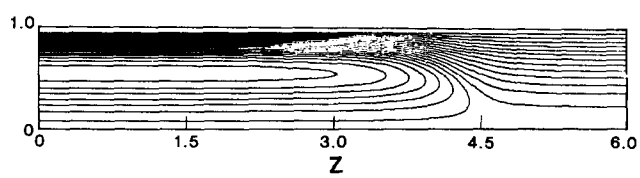

FIG. 3. A 2-D equilibrium with the Heaviside pressure profile $p(\psi) = CH(\psi)$.

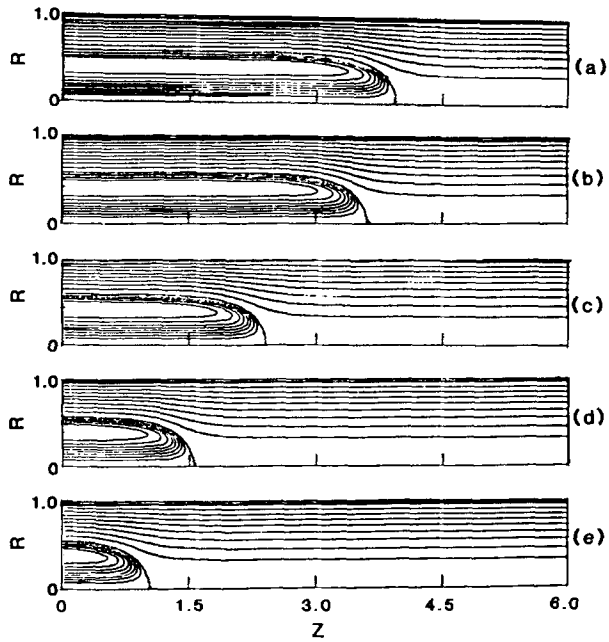

FIG. 4. A series of 2-D states for the SECH pressure profile for decreasing I_θ. The values of I_θ are (a) 24.0, (b) 22.0, (c) 15.0, (d) 10.0, and (e) 7.0.

(7) provide more freedom to find equilibria with characteristics similar to those observed in experiments.

A 1-D calculation exploiting the straight field lines at the midplane and at large values of z is used to choose these parameters (see Appendix).

It is convenient to classify these long equilibria by β_s, the pressure at the separatrix divided by the maximum pressure, and by x_s. Figure 4 displays the region in which long, $\epsilon \gg 1$, equilibria can be found with $p(\psi)$ given by Eq. (7); the corresponding a_1, b_1, d_1, and C for the desired β_s and x_s can be obtained by computing 1-D equilibria satisfying the average beta condition, as described in the Appendix. These pressure profile parameters are given in Table I for selected combinations of β_s and x_s. Taking $\beta_s = 0.1$ and $x_s = 0.6$ as a representative case, Figs. 4(a)–4(e) display a sequence of 2-D states for decreasing I_θ; the elongation ranges from $\epsilon = 6.7$ down to 1.67.

A typical case with a 40×80 mesh requires 150 iterations (30 CRAY CPU seconds) for $x_s = 0.59$, $\beta = 0.5$, and $\epsilon = 5.0$. Convergence is more rapid for larger x_s and smaller I_θ. An initial guess is made up of the 1-D plasma state for small z and the 1-D "vacuum-like" state for large z. A smooth transition between states is not attempted with the initial guess; the 1-D plasma state is used for $0 \leqslant z \leqslant I_\theta / J_\theta$ where J_θ is the current length of the 1-D plasma state and the 1-D vacuum-like state is abruptly used from $z = I_\theta / J_\theta$ out to $z = z_{\max}$.

Long 2-D states do not exist for combinations of x_s and β_s lying above or to the right of the dashed boundary in Fig. 5 because axial force balance cannot be achieved for such combinations. As this boundary is approached, the plasma near the axis at $z \gg z_s$ begins to exclude the magnetic field. When the boundary is reached B_{axis} (the magnetic field at $r = 0$ and $z \gg z_s$) goes to zero. Figure 6 shows what happens to the shape of an equilibrium as the boundary is approached. Equilibria (a) and (c) are well away from the boundary, while (b) is very near it. The needle-nosed shape of equilibrium (b) can be explained as follows. Consider the dashed line in equilibrium (c) of Fig. 6. It is constructed to be normal to the flux surfaces and to begin at the separatrix crossing on the z axis. Force balance normal to the flux surfaces is given by $\nabla_\perp (p + B^2/2) = B^2 \kappa$, where $\nabla_\perp$ is the gradient operator normal to a flux surface and where κ is the field line curvature vector. Integrating this equation along the dashed line, and using radial pressure balance for $z \gg z_s$, gives

$$\frac{B_{\text{axis}}^2 + B_t^2 - B_w^2}{2} = \int_0^{\text{wall}} B^2 \kappa \cdot d\mathbf{l}, \tag{8}$$

where B_t is the field on the dashed line at the wall and where B_w is the field at the wall for $z \gg z_s$. Note that $B_t \geqslant B_w$. This relation shows that as the equilibrium boundary is approached and B_{axis} decreases, the average curvature force on the dashed line decreases. The field lines then become

TABLE I. SECH equilibrium parameters.

β_s	x_s	a_1	b_1	d_1	C
0.01	0.40	383.77	2.298 6	5.389 7	101.12
0.01	0.50	138.32	2.300 4	4.896 4	50.504
0.01	0.60	58.833	2.304 1	4.470 8	30.892
0.01	0.70	23.412	2.311 9	4.085 0	22.675
0.01	0.80	9.367 0	2.327 8	3.720 0	20.640
0.01	0.90	2.949 2	2.360 4	3.358 7	27.674
0.01	0.96	0.869 03	2.311 7	3.010 4	58.915
0.20	0.40	170.64	0.699 19	3.015 6	81.032
0.20	0.50	58.230	0.710 39	2.497 0	42.709
0.20	0.60	21.744	0.737 39	2.039 2	28.114
0.20	0.70	8.179 3	0.802 47	1.618 6	23.567
0.20	0.79	3.204 7	0.936 85	1.278 7	27.670
0.40	0.40	108.85	0.220 62	2.132 3	74.138
0.40	0.50	33.943	0.258 67	0.920 04	41.244
0.40	0.60	11.051	0.365 14	1.099 4	30.997
0.40	0.66	5.642 3	0.499 88	0.859 55	32.191
0.60	0.40	60.756	−0.136 19	1.296 7	70.914
0.60	0.52	11.386	0.104 97	0.644 14	46.704

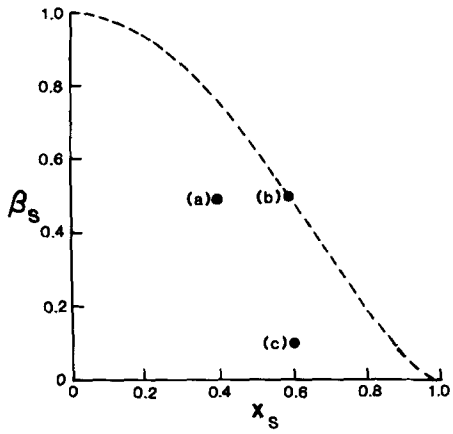

FIG. 5. Accessible parameter space for SECH pressure profile. Elongated equilibria cannot exist above and to the right of the dashed curve due to loss of axial pressure balance. Points indicate equilibria shown in Fig. 6.

straighter, causing B_t to approach B_w, so that the curvature force along the dashed line goes to zero at the equilibrium boundary. When zero curvature is reached, z_s goes to infinity and the field-reversed equilibrium is lost.

V. CONCLUSION

Elongated field-reversed equilibria similar to those observed in experiment have been difficult to compute. Recent work on the simplified Heaviside profile $p(\psi) = C\psi H(\psi)$ pointed to the extreme sensitivity of the elongation to subtle changes in the pressure function. Further consideration of the properties of this profile suggested the adoption of the total toroidal current I_θ as a less delicate means of specifying equilibria. Using this concept together with an adaptive elliptic solution technique for the Grad–Shafranov equation now allows routine solution to be achieved for states with arbitrary elongation.

Solutions with more general pressure profiles proved to have properties that are quite similar to solutions with the Heaviside profile. Exploiting this similarity, elongated equilibria were computed from pressure profiles that have sufficient generality to match experimentally measured quantities. As with the Heaviside profile, the z position of the separatrix is controlled by the amount of I_θ the configuration is required to have.

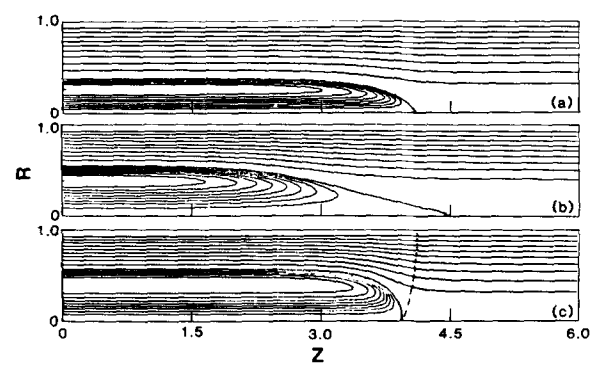

FIG. 6. Typical 2-D equilibria for the SECH pressure profile showing the change in shape that occurs as the axial force balance boundary is approached. (a) $\beta_s = 0.5$, $x_s = 0.4$, (b) $\beta_s = 0.5$, $x_s = 0.6$, and (c) $\beta_s = 0.1$, $x_s = 0.6$. The dashed line is perpendicular to flux surfaces; see Sec. IV. Case (a) is typical of FRC's produced by the FRX-C experiment at Los Alamos National Laboratory.

Examples were presented that exhibit the dependence of the elongation on I_θ. In addition, the more general $p(\psi)$ profiles exhibited a new property. For these profiles with given plasma beta on the separatrix, elongated two-dimensional equilibria can only be found for states having x_s less than a maximum permissible x_s. As β_s is increased the upper limit on permissible x_s is reduced.

ACKNOWLEDGMENTS

The authors acknowledge several useful discussions with R. S. Christian.

This work was performed under the auspices of the U.S. Department of Energy.

APPENDIX: ONE-DIMENSIONAL EQUILIBRIUM

A one-dimensional equilibrium calculation is described that makes it easy to choose pressure profiles that will produce two-dimensional equilibria with desired properties. It is based on the so-called "long-thin approximation"[1,11] and depends on having straight field lines in the midplane and at large values of z; 1-D equilibrium problems are solved in these two regions. The simplest way to compute equilibria depending only on the radial coordinate r is to choose $p(r)$ and to use $p + B_z^2/2 = \text{const}$ to find $B_z(r)$. Note that there is no toroidal field. This method is inappropriate here, however, because $p(\psi)$ is needed in the two-dimensional calculation. For this reason ψ is used as the independent variable; it is also convenient to normalize ψ to the trapped flux, i.e., to the value of ψ at the equilbrium O point. The pressure profile is chosen to be of the form

$$p(\psi) = (C\psi_w\psi_0/r_w^4)[\, g(\phi\,) - g(-\kappa)], \tag{A1}$$

where ψ_w is the value of the flux function at the wall, where ψ_0 is the value of ψ at the O point, where $\kappa = \psi_w/\psi_0$, and where $\phi = \psi/\psi_0$. The function g gives the shape of the pressure profile; C gives its magnitude. If the radial coordinate $\xi = (r/r_w)^2$ is used, then the magnetic field is given by

$$B_z(\xi\,) = \frac{2\psi_0}{r_w^2}\frac{d\phi}{d\xi}. \tag{A2}$$

Two different one-dimensional equilibria are of interest: (1) a field-reversed equilibrium to represent the midplane of a long field-reversed configuration and (2) a nonreversed equilibrium to represent the same configuration far away from the region of reversed field. Because these two regions are connected by a two-dimensional transition region, $p(\psi)$ must be the same for both, if the flow along the open field lines does not substantially alter the pressure. Available experimental evidence suggests that it does not.[1] Radial pressure balance for equilibrium (1) is given by

$$(\phi_1')^2 = [\, g(1) - g(\phi_1)]/\alpha^2, \tag{A3}$$

where $\alpha^{-1} = (C\psi_w/2\psi_0)^{1/2}$ and where $'$ means $d/d\xi$. Integrating Eq. (A3) from the axis to the wall gives a relation between α and κ,

$$\alpha[2\Delta + \Gamma(\kappa)] = 1, \tag{A4}$$

where

$$\Delta = \int_0^1 \frac{dy}{[\,g(1) - g(y)\,]^{1/2}}, \tag{A5}$$

$$\Gamma(\kappa) = \int_0^{\kappa} \frac{dy}{[\,g(1) - g(-y)\,]^{1/2}}. \tag{A6}$$

Radial pressure balance for equilibrium (2) is given by

$$(\phi_2')^2 = \alpha[\,\bar{g} - g(\phi_2)\,], \tag{A7}$$

where $\bar{g}$ is a constant. Integrating Eq. (A7) from the axis to the wall gives a relation between α, κ, and $\bar{g}$,

$$\alpha\Omega(\kappa,\bar{g}) = 1, \tag{A8}$$

where

$$\Omega(\kappa,\bar{g}) = \int_0^{\kappa} \frac{dy}{[\,\bar{g} - g(-y)\,]^{1/2}}. \tag{A9}$$

In order for these two equilibria to represent the midplane and the end of a two-dimensional field-reversed configuration, the axial equilibrium condition (average-beta condition)[1,11] must be satisfied. This condition can be written in the form

$$\frac{8}{r_w^2(B_{w1}^2 - B_{w2}^2)} \int_0^{r_w} (p_1 - p_2) r\,dr = 1, \tag{A10}$$

where B_{w1} and B_{w2} are the magnetic fields at the wall for the two equilibria. Equation (A10) can be rewritten for the present case as

$$\frac{\Lambda_1 - \Lambda_2}{g(1) - \bar{g}} = \frac{1}{2\alpha}, \tag{A11}$$

where

$$\Lambda_1 = 2\int_0^1 \frac{g(y) - g(-\kappa)}{[\,g(1) - g(y)\,]^{1/2}}\,dy + \int_0^{\kappa} \frac{g(-y) - g(-\kappa)}{[\,g(1) - g(-y)\,]^{1/2}}\,dy, \tag{A12}$$

and where

$$\Lambda_2 = \int_0^{\kappa} \frac{g(-y) - g(-\kappa)}{[\,\bar{g} - g(-y)\,]^{1/2}}\,dy. \tag{A13}$$

Equations (A4), (A8), and (A11) provide three relations to determine the three unknown quantities C, ψ_0, and $\bar{g}$, or equivalently, α, κ, and $\bar{g}$. Once these have been determined, Eqs. (A3) and (A7) can be integrated to find $\phi_1(r)$ and $\phi_2(r)$ and hence any other desired functions of radius. This solves the problem of finding the equilibrium produced by a given shape function g.

A useful addition to this calculation is to choose a shape function with free parameters in it and to simultaneously adjust these parameters to make the equilibrium have certain desired properties. For instance, it is useful to be able to produce equilibria having specified values of x_s and β_s. These two are given by

$$x_s = (2\alpha\Delta)^{1/2}, \tag{A14}$$

$$\beta_s = \frac{g(0) - g(-\kappa)}{g(1) - g(-\kappa)}. \tag{A15}$$

Choosing the shape function

$$g(\phi) = \tanh[\lambda(\phi - \phi^*)], \tag{A16}$$

the parameters λ and ϕ^* are to be determined along with the three equilibrium constants. Note that Eqs. (A4), (A8), and (A11) are linear in α; eliminating α leaves only four nonlinear equilibrium equations to solve for the four quantities κ, $\bar{g}$, λ, and ϕ^*. Their solution is accomplished by numerically evaluating the required definite integrals and by using the IMSL n-variable zero-finder ZSCNT. Once these constants have been found, they can be used to obtain a pressure profile for use in the two-dimensional equilibrium code. For instance, Eqs. (1), (A16), and (7) can be used to obtain the following relations between λ, ϕ^*, ψ_0, a_1, b_1, and d_1;

$$a_1 = \lambda/\psi_0, \tag{A17a}$$

$$b_1 = \lambda\phi^*, \tag{A17b}$$

$$d_1 = \psi_w\lambda/r_w^4. \tag{A17c}$$

Since the two-dimensional equilibrium code uses toroidal current as a constraint, it is useful to have expressions for the toroidal current per unit length in these one-dimensional equilibria. They are given by

$$J_1 = (C\psi_w/r_w^2)\alpha\{[\,g(1) - g(0)\,]^{1/2} + [\,g(1) - g(-\kappa)\,]^{1/2}\}, \tag{A18}$$

$$J_2 = (C\psi_w/r_w^2)\alpha\{[\,\bar{g} - g(-\kappa)\,]^{1/2} - [\,\bar{g} - g(0)\,]^{1/2}\}. \tag{A19}$$

Since this computation only involves performing definite integrals and finding zeroes of nonlinear equations, it provides a very rapid method of investigating many pressure profiles to determine their suitability for use in the two-dimensional equilibrium code.

[1] W. T. Armstrong, R. K. Linford, J. Lipson, D. A. Platts, and E. G. Sherwood, Phys. Fluids **24**, 2068 (1981).
[2] A. G. Es'kov, R. Kh. Kurtmullaev, Ya. N. Laukhin, A. I. Malyutin, A. I. Markin, Yu. S. Martyushov, B. N. Mironov, M. M. Orlov, A. P. Proshletsov, V. M. Semenov, and Ya. B. Sosunov, in *Plasma Physics and Controlled Nuclear Fusion Research* (IAEA, Vienna, 1978), Vol. II, p. 187.
[3] W. T. Armstrong, D. G. Harding, E. A. Crawford, and A. L. Hoffman, Phys. Fluids **25**, 2121 (1982).
[4] S. O. Knox, H. Meuth, F. L. Ribe, and E. Sevillano, Phys. Fluids **25**, 262 (1982).
[5] K. Hirano (private communication).
[6] S. Kaneko, K. Chiyoda, and I. Hirota, J. Phys. Soc. Jpn. **50**, 359 (1981).
[7] H. L. Berk, J. H. Hammer, and H. Weitzner, Phys. Fluids **24**, 1758 (1981).
[8] D. V. Anderson, J. H. Hammer, and D. C. Barnes, in *Proceedings of the Fourth Symposium on the Physics and Technology of Compact Toroids* (LLNL, Livermore, CA, 1981).
[9] V. N. Semenov and N. V. Sosnin, Fiz. Plasmy 7, 333 (1981) [Sov. J. Plasma Phys. 7, 180 (1981)].
[10] R. L. Spencer and D. W. Hewett, Phys. Fluids **25**, 1365 (1981).
[11] D. C. Barnes, C. E. Seyler, and D. V. Anderson, in *Proceedings of the US-Japan Joint Symposium on Compact Toruses and Energetic Particle Injection* (PPL, Princeton, NJ, 1979), p. 110.
[12] B. Marder and H. Weitzner, Plasma Phys. **12**, 435 (1970).
[13] S. Doss and K. Miller, SIAM J. Numer. Anal. **16**, 837 (1979).
[14] D. Henning (private communication).